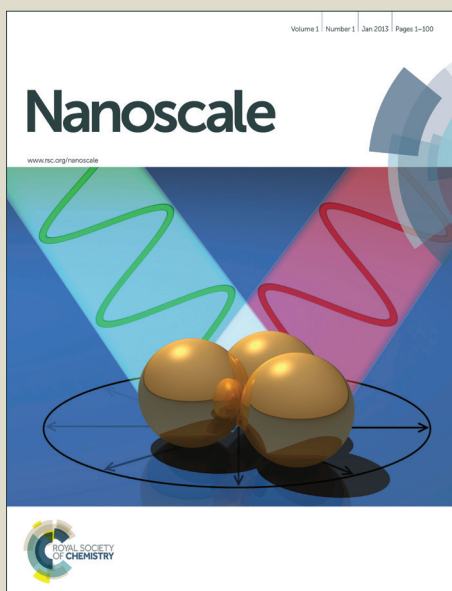


# Nanoscale

Accepted Manuscript



This is an *Accepted Manuscript*, which has been through the Royal Society of Chemistry peer review process and has been accepted for publication.

*Accepted Manuscripts* are published online shortly after acceptance, before technical editing, formatting and proof reading. Using this free service, authors can make their results available to the community, in citable form, before we publish the edited article. We will replace this *Accepted Manuscript* with the edited and formatted *Advance Article* as soon as it is available.

You can find more information about *Accepted Manuscripts* in the [Information for Authors](#).

Please note that technical editing may introduce minor changes to the text and/or graphics, which may alter content. The journal's standard [Terms & Conditions](#) and the [Ethical guidelines](#) still apply. In no event shall the Royal Society of Chemistry be held responsible for any errors or omissions in this *Accepted Manuscript* or any consequences arising from the use of any information it contains.

## Topological insulator states in a honeycomb lattice of s-triazines

Aizhu Wang, Xiaoming Zhang, Mingwen Zhao\*

*School of Physics and State Key Laboratory of Crystal Materials, Shandong  
University, Jinan 250100, Shandong, China*

### Abstract

Two-dimensional (2D) graphitic carbon nitride materials have been drawing an increasing attention in energy conversion, environment protection and spintronic devices. Here, based on first-principles calculations, we demonstrate that the already-synthesized honeycomb lattice of s-triazines with a chemical formula of  $C_6N_6$  (g- $C_6N_6$ ) has topologically nontrivial electronic states characterized by  $p_{x,y}$ -orbital band structures with a topological invariant of  $Z_2=1$ , and stronger spin-orbital coupling (SOC) than both graphene and silicene. The band gaps opened in the  $p_{x,y}$ -orbital bands due to SOC are 5.50 meV (K points) and 8.27 eV ( $\Gamma$  point), respectively, implying that quantum spin Hall effect (QSHE) could be achieved in this 2D graphitic carbon nitride material at the temperature lower than 95 K. This offers a viable approach for searching for 2D Topological Insulators (TIs) in metal-free organic materials.

\*E-mail: [zmw@sdu.edu.cn](mailto:zmw@sdu.edu.cn)

†Electronic supplementary information (ESI) available: Ruby model and the relevant tight-binding Hamiltonian, parity tables for the g- $C_6N_6$  lattice and the corresponding  $Z_2$  invariants, phonon spectra of g- $C_{12}N_6$  and g- $C_{24}N_6H_{12}$  lattices.

## Introduction

Topological Insulators (TIs), a newly discovered quantum class of materials with topological order<sup>1,2</sup>, have become an exciting subject of intensive research not only in fundamental and applied branches of condensed matter physics<sup>3, 4</sup>, but also in solid-state chemistry and materials science<sup>5</sup>. TIs are the materials with a bulk band gap generated by strong spin-orbit coupling (SOC) and topologically protected metallic surface states. Some unique properties, such as magnetic monopole<sup>6</sup>, Majorana fermions<sup>7</sup>, novel magnetoelectrics<sup>8</sup>, charge fractionalization<sup>9</sup>, and quantum anomalous Hall effect<sup>10</sup> have been proposed, which are quite promising for the uses of quantum computing<sup>11</sup> and spintronic devices<sup>12</sup>. To date, HgTe and Bi<sub>2</sub>Se<sub>3</sub> are the two large families of TIs, as revealed by both theoretical and experimental works<sup>1, 2, 13, 14</sup>.

Among the TIs, two-dimensional (2D) TIs are ideally suitable for above applications due to the robustness of conducting edge states from backscattering, so searching for 2D TIs is an exciting topic. Graphene was the first material predicted to realize TI<sup>15</sup>, where SOC opens a band gap at the Dirac points. Quantum spin Hall effect (QSHE), a new quantum state of matter with a nontrivial topological property, was firstly expected to be achieved in graphene. However, subsequent works indicated that the SOC gap is unobservable small (approximately  $10^{-3}$  meV) due to the very weak SOC in graphene<sup>16</sup> and the QSHE can only occur at an unrealistically low temperature<sup>16, 17</sup>. Further theoretical works suggest that the SOC gap of graphene can be dramatically enhanced to detectable values by dilute concentrations of *3d* or *5d* transition metal adatoms<sup>18, 19</sup>, which can host quantum spin Hall states or quantum anomalous Hall states. Topological insulator states have also been predicted in Bi (111) films and many metal-organic frameworks with remarkable SOC<sup>20-24</sup>. However, the topological insulator states and the QSHE in 2D metal-free organic frameworks remain unclear. Although, SOC is always very weak for light elements, it can be substantially enhanced by arranging light atoms in special ways, as revealed in  $\delta$ -graphyne<sup>25</sup>.

Graphitic carbon nitride (g-C<sub>3</sub>N<sub>4</sub>) is another 2D organic material family, which has

been studied for more than one hundred years<sup>26</sup>. The interests in polymeric graphitic carbon nitride materials were aroused recently owing to their potential applications in fuel cells, photocatalysis, and hydrogen production<sup>27-29</sup>. There are two prevailing models of g-C<sub>3</sub>N<sub>4</sub>. One has triazine (C<sub>3</sub>N<sub>3</sub>) as building blocks (referred to as s-triazine) as shown in Fig. 1(a), while the building blocks of another model, tri-s-triazine (heptazine) rings, resemble the hypothetical polymer melon<sup>30,31</sup>, both of which have the chemical formula of C<sub>3</sub>N<sub>4</sub>. These g-C<sub>3</sub>N<sub>4</sub> materials are semiconductors with trivial band gaps of 1.16 eV and 0.89 eV<sup>32</sup>.

Interestingly, theoretical works indicate that when parts of nitrogen atoms are replaced by carbon atoms, the graphitic carbon nitride materials (g-C<sub>3</sub>N<sub>4</sub>) convert to spin-polarized semiconductors or half-metals<sup>33, 34</sup>, which broadens the fields of application, *e.g.* spintronic devices. However, topological insulator states have never been predicted in those carbon nitride materials up to now. In this contribution, we demonstrated theoretically that a honeycomb lattice of s-triazines (Fig. 1(b)) has topologically nontrivial electronic states in the  $p_{x,y}$ -orbital bands with a topological invariant of  $Z_2=1$ . This 2D carbon nitride material with a chemical formula of C<sub>6</sub>N<sub>6</sub> per primitive cell (denoted as g-C<sub>6</sub>N<sub>6</sub>), as shown in Fig. 1(b), has superior stability and thus high plausibility in experiments. More interestingly, the SOC in this metal-free organic material is much stronger than that in graphene<sup>16</sup> and silicene<sup>35</sup>. The SOC gaps opened in the  $p_{x,y}$ -orbital bands are 5.50 meV at K points and 8.27 meV at  $\Gamma$  point in Brillouin Zone (BZ), respectively, suggesting that QSHE may be achieved in the g-C<sub>6</sub>N<sub>6</sub> lattice at the temperature lower than 95 K. Our study offers an ideal candidate material for the long-desired 2D counterpart of honeycomb lattice featured by the interesting properties of both flat bands and Dirac cones, which are quite promising to realize fractional quantum Hall effects<sup>36</sup>.

## Method and Computational Details

Our first-principles calculations were performed within the framework of density-functional theory (DFT), which is implemented in the Vienna ab initio simulation package known as VASP<sup>37</sup>. The electron-electron interactions were treated

using a generalized gradient approximation (GGA) in form of Perdew-Burke-Ernzerhof (PBE) for the exchange-correlation functional<sup>38</sup>. The energy cutoff employed for plane-wave expansion of electron wavefunctions was set to 520 eV. The electron-ion interactions were described by projector-augmented-wave (PAW) potentials<sup>39</sup>. Four electrons for carbon ( $2s^22p^2$ ) and five electrons for nitrogen ( $2s^22p^3$ ) were treated as valence electrons. The supercells were repeated periodically on the x-y plane while a vacuum region of 20 Å was applied along the z-direction to avoid mirror interactions between neighboring images. The BZ integration was sampled on a grid of  $15 \times 15 \times 1$  k-points. Structural optimizations were carried out using a conjugate gradient (CG) method until the remaining force on each atom was less than 0.001 eV/Å.

## Results and discussion

Figure 1(b) gives the optimized configuration of g-C<sub>6</sub>N<sub>6</sub> lattice. The atomic structure of g-C<sub>3</sub>N<sub>4</sub> is also presented for the purpose of comparison. Different from g-C<sub>3</sub>N<sub>4</sub>, the s-triazines in g-C<sub>6</sub>N<sub>6</sub> are joined together via C-C bonds without the need of additional nitrogen atoms, leading to a honeycomb lattice with a chemical formula of C<sub>6</sub>N<sub>6</sub> per primitive cell. Planar configuration and the six-fold symmetry are well preserved in g-C<sub>6</sub>N<sub>6</sub> lattice. The C-N bond length in the s-triazine rings is 1.340 Å, which is longer than that in g-C<sub>3</sub>N<sub>4</sub> (1.327 Å). The C-N-C bond angle, 114.4°, deviates slightly from the bond angle in graphene, 120°. The C-C bond length between adjacent s-triazines is 1.509 Å, longer than that in graphene (1.420 Å). This may be related to the polarization of the dangling bond electrons by the local strain and quantum entrapment of the core and bonding electrons at the edges<sup>40</sup>.

We tested the stability of the g-C<sub>6</sub>N<sub>6</sub> framework using three strategies. First, we evaluated the energetic stability with respect to g-C<sub>3</sub>N<sub>4</sub>, which has been realized experimentally<sup>41</sup>. Because they have different stoichiometries, the energetic stability is dependent on the chemical potentials of carbon ( $\mu_C$ ) and nitrogen ( $\mu_N$ ) atoms. Here, we defined the formation energy ( $\Delta E$ ) as:

$$\Delta E = \left[ E_{total} [C_xN_y] - x\mu_C - y\mu_N \right] / (x + y)$$

where  $E_{total}$  represents the total energy of graphitic carbon nitride materials with a stoichiometry of  $C_xN_y$ ,  $\mu_C$  and  $\mu_N$  are the chemical potentials of carbon and nitrogen atoms. Under carbon-rich conditions,  $\mu_C$  was calculated from graphene. Under nitrogen-rich condition,  $\mu_N$  was calculated from a  $N_2$  molecule in gas phase. In both cases,  $\mu_C$  and  $\mu_N$  were linked by the thermodynamic constraint,  $3\mu_C + 4\mu_N = E_{g-C_3N_4}$ , where  $E_{g-C_3N_4}$  is the total energy of a  $C_3N_4$  unit in g- $C_3N_4$ . The formation energies of g- $C_4N_3$  and g- $C_6N_6$  are listed in Table 1. Although the value of formation energy depends on the definition itself<sup>42</sup>, the negative formation energies of the g- $C_6N_6$  framework suggest its high plausibility. Secondly, we calculated the phonon spectrum of the g- $C_6N_6$  framework to test its kinetic stability. The phonon spectrum was calculated by the force-constant theory combined with the VASP code. The phonon dispersion relations along high-symmetric directions in BZ were plotted in Fig. 1(c). Clearly, the phonon spectrum is free from imaginary frequencies, suggesting that the g- $C_6N_6$  framework is kinetically stable. The optical and acoustical branches are well separated in the spectrum. Two acoustical branches have linear dispersion relations near the center of BZ ( $\Gamma$  point). It is noteworthy that the transverse acoustical phonon branch has no imaginary frequencies near the  $\Gamma$  point in contrast with the cases of germanium silicide<sup>43</sup> and siligraphenes<sup>44</sup>. This suggests that the g- $C_6N_6$  framework is stable for the particular mode with long wavelength. Finally, we performed molecular dynamics (MD) simulations using a large supercell ( $5 \times 5$ ) of g- $C_6N_6$  at room temperature ( $T = 300$  K) for 1 ps. Our MD simulations clearly indicate that geometry of g- $C_6N_6$  remains unchanged in addition to small fluctuations of temperature and total energy with the passage of time. Although the time scale is too short due to the computational limitation, our MD results imply that the g- $C_6N_6$  framework is stable at room temperature. The stability and plausibility of the g- $C_6N_6$  framework have also been confirmed experimentally. By the reactions of cyanuric chloride with sodium metal, as shown in Fig. 1(d), a layered  $sp^2$ -bonded structure composed of s-triazine rings bridged by carbon-carbon bonds has been synthesized<sup>45, 46</sup>. This layered material

can be regarded as g-C<sub>6</sub>N<sub>6</sub> multilayers.

Because X-ray diffraction (XRD) spectra are quite useful for characterization of novel synthesized materials, we simulated the XRD spectrum of the g-C<sub>6</sub>N<sub>6</sub> framework with a wavelength of 1.540562 Å. The XRD spectra of the already-synthesized g-C<sub>3</sub>N<sub>4</sub><sup>34</sup> and g-C<sub>4</sub>N<sub>3</sub> lattices were also presented for the purpose of comparison. It is clear that these three materials have sharp peaks at  $2\theta=8.84^\circ$ ,  $13.27^\circ$  and  $17.72^\circ$ , corresponding to their (002), (003) and (004) planes as showed in Fig. 2. However, g-C<sub>6</sub>N<sub>6</sub> has additional peaks at  $2\theta=14.35^\circ$ ,  $15.03^\circ$ ,  $16.88^\circ$  and  $19.59^\circ$ , which can be regarded as fingerprints to identify the g-C<sub>6</sub>N<sub>6</sub> from other graphitic carbon nitride materials.

We then turn to the electronic structures of g-C<sub>6</sub>N<sub>6</sub> lattice. The electronic band structures obtained from first-principles calculations indicate that it is a nonmagnetic semiconductor with a band gap of 1.53 eV, as shown in Fig. 3(a). Interestingly, we can see the typical signature of  $p_{x,y}$ -orbital band structures in the honeycomb lattice<sup>36</sup>, which composes of two Dirac bands sandwiched by two flat bands in the valence band region near the Fermi level. Without SOC, the two Dirac bands meet in a single point at six highly-symmetric points in BZ (K points). Around the meeting point, the Dirac bands are linear and can be characterized by Dirac cones. The charge carriers (electrons and holes) in these bands will behave as massless Dirac fermions. The slopes, *i.e.*, first derivatives of the band energies of the two Dirac bands in reciprocal space, are equal to  $\pm 7.7\text{eV}\text{\AA}$  compared to the values of  $\pm 35.2\text{eV}\text{\AA}$  in graphene<sup>47, 48</sup> along the  $\Gamma$ -K point. Additionally, the two flat bands touch the two Dirac bands at the  $\Gamma$  point, respectively. The energies at the meeting points ( $\Gamma$  and K points) are 0.451 eV and 0.870 eV below the Fermi level without doping as shown in Fig. 3(a). Such small energy difference may facilitate to move the Fermi level down to the meeting points by applying an electrostatic gating voltage.

The origins of the flat and Dirac bands were studied by analyzing the electron density of states (PDOS) projected onto different atomic orbitals, as shown in Fig. 3(b). From the figure, we can see clearly that the top four valence bands come mainly from the  $p_x$  and  $p_y$  orbitals of the nitrogen atoms on the basal plane, while the  $p_z$

orbitals mainly contribute to the three conduction bands near the Fermi level. This is also consistent with the isosurfaces of the Kohn-Sham wave functions plotted in Fig. 3(d).

Based on the above features, we adopted a simple tight-binding (TB) model to reproduce the four valence bands. In this model, we only consider the nearest-neighbor (NN) hopping between the in-plane  $p_{x,y}$  atomic orbitals of nitrogen atoms of the g-C<sub>6</sub>N<sub>6</sub> lattice, leading to a ‘nitrogen lattice’. According to this approximation, the TB Hamiltonian reads as:

$$H = \varepsilon \sum_{i\alpha} c_{i\alpha}^{\dagger} c_{i\alpha} + \sum_{\langle i,j \rangle, \alpha, \beta} t_{ij\alpha\beta} c_{i\alpha}^{\dagger} c_{j\beta} + \sum_{\langle\langle i,j \rangle\rangle, \alpha, \beta} \gamma_{ij\alpha\beta} c_{i\alpha}^{\dagger} c_{j\beta}$$

Here  $\alpha, \beta \in (p_x, p_y)$ ,  $\varepsilon$  is the on-site energy of  $p_{x,y}$ -orbitals,  $c_{i\alpha}^{\dagger}$  and  $c_{i\alpha}$  are the creation and annihilation operators of an  $\alpha$ -orbital electron at the  $i$ -th atom, respectively. The parameter  $t_{ij\alpha\beta}$  (or  $\gamma_{ij\alpha\beta}$ ) represents the NN hopping energy of an electron between the  $\alpha$ -orbital of  $i$ -th atom and the  $\beta$ -orbital of  $j$ -th atom within the same (different) s-triazine unit(s). Taking the interactions between different atomic orbitals into account, the hopping integrals are given as the following forms with  $t_{ij\alpha\beta} = E_{\alpha\beta}$  and  $\gamma_{ij\alpha\beta} = \eta E_{\alpha\beta}$ :

$$\begin{aligned} E_{p_x p_x} &= V_{pp\sigma} \times \cos^2 \theta + V_{pp\pi} \times \sin^2 \theta \\ E_{p_y p_y} &= V_{pp\sigma} \times \cos^2 \varphi + V_{pp\pi} \times \sin^2 \varphi \\ E_{p_x p_y} &= (V_{pp\sigma} - V_{pp\pi}) \times \cos \theta \times \cos \varphi \end{aligned}$$

The parameters  $\theta$  and  $\varphi$  are the angles of the vector pointing from  $i$ -th to  $j$ -th atoms with respect to  $x$ - and  $y$ -directions. The optimal values for the g-C<sub>6</sub>N<sub>6</sub> are  $\varepsilon = 0.50$  eV,  $\eta = 0.266$ ,  $V_{pp\sigma} = 1.504$  eV, and  $V_{pp\pi} = -1.303$  eV, respectively. With the above parameters, our TB Hamiltonian reproduces well the top four valence band of the g-C<sub>6</sub>N<sub>6</sub> given by DFT calculations, as shown in Fig. 3(a). This confirms that the four bands of the g-C<sub>6</sub>N<sub>6</sub> are  $p_{x,y}$ -orbital bands<sup>36</sup>. The slight deviation of the TB model to the DFT data can be attributed to the small contribution of the  $s$  orbital of nitrogen and the atomic orbitals of carbon atoms, which are omitted in this TB Hamiltonian. It is noteworthy that the  $p_{x,y}$ -orbital band structures has been proposed as a promising

model system to achieve fractional quantum Hall effect<sup>20</sup>, but has been realized in rare systems. Our work, however, offers a promising candidate material to reach this goal.

Interestingly, the Kohn-Sham wavefunctions of g-C<sub>6</sub>N<sub>6</sub> shown in Fig. 3(d) exhibit noticeable features of a ruby lattice<sup>49</sup>. Actually, the top four valence bands ( $p_{x,y}$ -orbital bands) can also be reproduced using a TB Hamiltonian of ruby lattices. More details can be seen in the ESI†.

Finally, we investigated the SOC effects on the electronic structures of the g-C<sub>6</sub>N<sub>6</sub> framework. As a benchmark, we first calculated the SOC gap in graphene and found that it is only 0.008 meV, close to the value reported in previous works<sup>25</sup>. For the g-C<sub>6</sub>N<sub>6</sub> lattice, SOC opens two band gaps in the four  $p_{x,y}$ -orbital bands, as shown in Fig. 3(c). One is between the two Dirac bands at K points, which is 5.50 meV. The other appears between the top flat band and second highest valence band (top Dirac band) at  $\Gamma$  point, which is 8.27 meV. Both are much larger than that in graphene<sup>16</sup> and silicene<sup>35</sup>. The SOC in graphene is in fact a second order process because the Dirac bands are contributed by the  $p_z$  orbital normal to graphene plane<sup>16</sup>. Therefore, graphene is not an ideal system to investigate orbital physics<sup>36</sup>. For the g-C<sub>6</sub>N<sub>6</sub>, however, the flat and Dirac bands arise mainly from the  $p_{x,y}$  orbitals in the basal plane with orbital degeneracy and spatial anisotropy, and the SOC gaps appear directly from the onsite term, leading to larger SOC gaps than that in graphene.

In order to determine topological features, we used the parity criteria proposed by Fu and Kane<sup>7</sup> to calculate the  $Z_2$  topological index. The  $Z_2$  index is determined by the parity of occupied bands on each time-reversal invariant momentum. In this strategy, the  $Z_2$  invariant  $\nu$  is defined by

$$(-1)^\nu = \prod_i \delta_i \text{ with } \delta_i = \prod_{m=1}^N \xi_{2m}(\Gamma_i)$$

for  $2N$  occupied bands.  $\xi_{2m}(\Gamma_i) = \pm 1$  is the parity eigenvalue of the  $2m$ -th occupied energy bands at the time-reversal invariant momentum  $\Gamma_i$ . The two states of a Kramers doublet have the same parity,  $\xi_{2m} = \xi_{2m-1}$ . It means that with inversion symmetry, the  $Z_2$  topological invariants can be deduced from the knowledge of the

parities of the four time-reversal and parity invariant points at BZ. This provides a simple method for determining the topological phases of the lattices with inversion symmetry, without having to know about the global properties of the energy bands. For the g-C<sub>6</sub>N<sub>6</sub> lattice, the four time-reversal invariant momenta occur at  $\Gamma_{i=(n_1, n_2)} = (n_1 \bar{b}_1 + n_2 \bar{b}_2) / 2$  with  $n_1, n_2 = 0, 1$  and  $\bar{b}_1, \bar{b}_2$  are primitive reciprocal lattice vectors, which correspond to the  $\Gamma$  and three M points in BZ, as shown in Fig.4. The parities of a band at the four time-reversal momenta can be determined from the corresponding electron wavefunctions given by first-principle calculations. More details can be found in the ESI†. We calculated the  $\delta_i$  values for the SOC gaps opened at the  $\Gamma$  ( $\Delta_1$ ) and K ( $\Delta_2$ ) points, as shown in Fig. 4. The parities of the relevant bands, as well as the  $\delta_i$  values at the four time-reversal momenta are listed in the ESI†. The topological invariants corresponding to the two SOC gaps are  $Z_2=1$ , implying the topologically nontrivial electronic structures of the g-C<sub>6</sub>N<sub>6</sub> lattice. The topological invariants of the g-C<sub>6</sub>N<sub>6</sub> framework calculated from the Kohn-Sham wavefunctions are in good agreement with those from the TB model of a ruby lattice<sup>48</sup>. The topological properties of the four  $p_{x,y}$ -orbital bands have been carefully studied in previous literatures<sup>20, 50</sup> based on a theoretically designed organometallic framework. Our work suggests that the experimentally accessible honeycomb lattice of s-triazines also has the same features, except that the SOC gaps in this metal-free material are rather smaller than that in the organometallic framework.

It should also be noticed that, the Fermi level of the g-C<sub>6</sub>N<sub>6</sub> is not in the SOC gaps, so doping is needed. Partial doping may lead to exotic fractional topological states. We considered two types of doping in this work. Doping two holes per unit cell moves the Fermi level to the SOC gap ( $\Delta_1$ ) and increases the SOC gap to 8.42 meV. This corresponds to a doping concentration of  $4.8 \times 10^{14} \text{ cm}^{-2}$ . In experiments, the doping effect can be achieved by the electrostatic gating. Recent experiment has demonstrated that the same order of doping concentration ( $4 \times 10^{14} \text{ cm}^{-2}$ ) in graphene can be achieved for both electrons and holes by using a solid polymer electrolyte gate<sup>51</sup>. Moving the Fermi level to the SOC gap between the two Dirac bands ( $\Delta_2$ )

requires a doping concentration of  $9.6 \times 10^{14} \text{ cm}^{-2}$  (four holes per unit cell). The SOC gap remains stable at this doping concentration.

Apart from the  $g\text{-C}_6\text{N}_6$  lattice, we also considered other honeycomb lattices of *s*-triazines jointed by acetylenic bonds or benzene rings with the chemical formulas of  $\text{C}_{12}\text{N}_6$  (referred to as  $g\text{-C}_{12}\text{N}_6$ ) and  $\text{C}_{24}\text{N}_6\text{H}_{12}$  (referred to as  $g\text{-C}_{24}\text{N}_6\text{H}_{12}$ ) per unit cell, as shown in Fig. 5(a) and 5(b), respectively. The two honeycomb lattices have perfect planar configurations with the lattice constants of 11.721 Å and 14.560 Å, respectively. The kinetic stability has also been confirmed by their phonon spectra, both of which are free from imaginary frequencies. More details can be found in the ESI†. For the four bands (two Dirac bands sandwiched by two flat bands) also appear in the electronic band structures of  $g\text{-C}_{12}\text{N}_6$  and  $g\text{-C}_{24}\text{N}_6\text{H}_{12}$  lattices. However, the slopes of the Dirac bands near the Dirac points are smaller than the corresponding value of  $g\text{-C}_6\text{N}_6$ , due to the large lattice constant. The SOC also opens band gaps between the top flat band and the top Dirac band at  $\Gamma$  point and the two Dirac bands at K points in  $g\text{-C}_{24}\text{N}_6\text{H}_{12}$  lattice. This confirms that the topologically nontrivial electronic states revealed in the  $g\text{-C}_6\text{N}_6$  lattice are the intrinsic properties of the honeycomb lattices of *s*-triazines.

## Conclusions

Using first-principles calculations combined with TB models, we demonstrated that the honeycomb lattice of *s*-triazines has superior stability and remarkable spin-orbital interactions. The valence bands in proximity of the Fermi level have the features of  $p_{x,y}$ -orbital bands composing of two Dirac bands sandwiched by two flat bands, which arise mainly from the  $p_x$  and  $p_y$  orbitals of nitrogen atoms. SOC opens band gaps of about 8.27 meV between the top flat band and the top Dirac band at  $\Gamma$  point and about 5.50 meV at K points between the two Dirac bands, leading to topologically nontrivial electronic states characterized by a topological invariant of  $Z_2=1$ . QSHE may be achieved in this 2D carbon nitride materials in an experimentally accessible low temperature region (<95 K). This can be regarded as the intrinsic features of the

honeycomb lattices of s-triazines, which provides a viable approach for searching for metal-free 2D TIs.

## Acknowledgements

This work is supported by the National Basic Research Program of China (No.2012CB932302), the National Natural Science Foundation of China (No.91221101), and National Super Computing Centre in Jinan.

## References

1. Y. L. Chen, J. G. Analytis, J. H. Chu, Z. K. Liu, S. K. Mo, X. L. Qi, H. J. Zhang, D. H. Lu, X. Dai, Z. Fang, S. C. Zhang, I. R. Fisher, Z. Hussain and Z. X. Shen, *Science*, 2009, **325**, 178-181.
2. D. Hsieh, D. Qian, L. Wray, Y. Xia, Y. S. Hor, R. J. Cava and M. Z. Hasan, *Nature*, 2008, **452**, 970-975.
3. B. A. Bernevig and S.-C. Zhang, *Phys. Rev. Lett.*, 2006, **96**, 106802.
4. L. Muechler, H. Zhang, S. Chadov, B. Yan, F. Casper, J. Kuebler, S.-C. Zhang and C. Felser, *Angew. Chem. Int. Ed.*, 2012, **51**, 7221-7225.
5. D. Kong and Y. Cui, *Nat. Chem.*, 2011, **3**, 845-849.
6. X.-L. Qi, R. Li, J. Zang and S.-C. Zhang, *Science*, 2009, **323**, 1184-1187.
7. L. Fu and C. Kane, *Phys. Rev. B*, 2009, **79**, 161408.
8. Q. Meng, V. Shivamoggi, T. L. Hughes, M. J. Gilbert and S. Vishveshwara, *Phys. Rev. B*, 2012, **86**, 165110.
9. B. Seradjeh, J. Moore and M. Franz, *Phys. Rev. Lett.*, 2009, **103**, 066402.
10. R. Yu, W. Zhang, H. J. Zhang, S. C. Zhang, X. Dai and Z. Fang, *Science*, 2010, **329**, 61-64.
11. M. Z. Hasan and C. L. Kane, *Rev. Mod. Phys.*, 2010, **82**, 3045-3067.
12. N. Nagaosa, *Science*, 2007, **318**, 758-759.
13. F. Yang, L. Miao, Z. F. Wang, M. -Y. Yao, F. Zhu, Y. R. Song, M. -X. Wang, J. -P. Xu, A. V. Fedorov, Z. Sun, G. B. Zhang, C. Liu, F. Liu, D. Qian, C. L.

- Gao and J. -F. Jia, *Phys. Rev. Lett.*, 2012, **109**, 016801.
14. T. Hirahara, G. Bihlmayer, Y. Sakamoto, M. Yamada, H. Miyazaki, S.-i. Kimura, S. Blügel and S. Hasegawa, *Phys. Rev. Lett.*, 2011, **107**, 166801.
  15. C. L. Kane and E. J. Mele, *Phys. Rev. Lett.*, 2005, **95**, 226802.
  16. Y. Yao, F. Ye, X.-L. Qi, S.-C. Zhang and Z. Fang, *Phys. Rev. B*, 2007, **75**, 041401.
  17. H. Min, J. E. Hill, N. A. Sinitsyn, B. R. Sahu, L. Kleinman and A. H. MacDonald, *Phys. Rev. B*, 2006, **74**, 165310.
  18. J. Hu, J. Alicea, R. Wu and M. Franz, *Phys. Rev. Lett.*, 2012, **109**, 266801.
  19. H. Zhang, C. Lazo, S. Bluegel, S. Heinze and Y. Mokrousov, *Phys. Rev. Lett.*, 2012, **108**, 056802.
  20. Z. Liu, Z.-F. Wang, J.-W. Mei, Y.-S. Wu and F. Liu, *Phys. Rev. Lett.*, 2013, **110**, 106804.
  21. M. Zhao, A. Wang and X. Zhang, *Nanoscale*, 2013, **5**, 10404-10408.
  22. Z. F. Wang, Z. Liu and F. Liu, *Phys. Rev. Lett.*, 2013, **110**, 196801.
  23. Z. F. Wang, N. Su and F. Liu, *Nano lett.*, 2013, **13**, 2842-2845.
  24. Z. F. Wang, Z. Liu and F. Liu, *Nature Commun.* 2013, **4**, 1471.
  25. M. Zhao, W. Dong and A. Wang, *Sci. Rep.*, 2013, **3**, 3532.
  26. E. C. Franklin, *J. Am. Chem. Soc.*, 1922, **5**, 486.
  27. A. Du, S. Sanvito, Z. Li, D. Wang, Y. Jiao, T. Liao, Q. Sun, Y. H. Ng, Z. Zhu, R. Amal and S. C. Smith, *J. Am. Chem. Soc.*, 2012, **134**, 4393-4397.
  28. L. Ge, F. Zuo, J. Liu, Q. Ma, C. Wang, D. Sun, L. Bartels and P. Feng, *J. Phys. Chem. C*, 2012, **116**, 13708-13714.
  29. Y. Zheng, J. Liu, J. Liang, M. Jaroniec and S. Z. Qiao, *Energ. Environ. Sci.* 2012, **5**, 6717-6731.
  30. Y. Wang, X. Wang and M. Antonietti, *Angew. Chem. Int. Ed.*, 2012, **51**, 68-89.
  31. J. Sehnert, K. Baerwinkel and J. Senker, *J. Phys. Chem. B*, 2007, **111**, 10671-10680.
  32. Y. Xu and S.-P. Gao, *Int. J. Hydrogen Energ.*, 2012, **37**, 11072-11080.

33. A. Du, S. Sanvito and S. C. Smith, *Phys. Rev. Lett.*, 2012, **108**, 197207.
34. X. Zhang, M. Zhao, A. Wang, X. Wang and A. Du, *J. Mater. Chem. C*, 2013, **1**, 6265.
35. C. -C. Liu, W. Feng and Y. Yao, *Phys. Rev. Lett.*, 2011, **107**, 076802.
36. C. Wu and S. Das Sarma, *Phys. Rev. B*, 2008, **77**, 235107.
37. G. Kresse and J. Furthmuller, *Phys. Rev. B*, 1996, **54**, 11169-11186.
38. J. P. Perdew, K. Burke, *Phys. Rev. Lett.*, 1997, **78**, 1396.
39. G. Kresse and D. Joubert, *Phys. Rev. B*, 1999, **59**, 1758.
40. C. Q. Sun, *Springer series of Chem Phys.*, Relaxation of the Chemical bond, part II, 2014, **108**, 239-249.
41. E. Kroke, M. Schwarz, E. Horath-Bordon, P. Kroll, B. Noll and A. D. Norman, *New J. Chem.*, 2002, **26**, 508-512.
42. A. Wang, M. Zhao, Y. Xi, X. Wang and Z. Wang, *Phys. Lett. A*, 2013, **377**, 1102-1108.
43. H. Zhou, M. Zhao, X. Zhang, W. Dong, X. Wang, H. Bu and A. Wang, *J. Phys.: Condens. Mat.*, 2013, **25**, 395501.
44. M. Zhao and R. Zhang, *Phys. Rev. B*, 2014, **89**, 195427.
45. T. Mu, J. Huang, Z. Liu, B. Han, Z. Li, Y. Wang, T. Jiang and H. Gao, *J. Mater. Res.*, 2004, **19**, 1736-1741.
46. J. Li, C. Cao, J. Hao, H. Qiu, Y. Xu and H. Zhu, *Diam. Relat. Mater.*, 2006, **15**, 1593-1600.
47. D. Malko, C. Neiss, F. Vines and A. Goerling, *Phys. Rev. Lett.*, 2012, **108**, 086804.
48. A. Wang, L. Li, X. Wang, H. Bu and M. Zhao, *Diam. Relat. Mater.*, 2014, **41**, 65-72.
49. X. Hu, M. Kargarian and G. A. Fiete, *Phys. Rev. B*, 2011, **84**, 155166.
50. W. Li, Z. Liu, Y.-S. Wu and Y. Chen, *Phys. Rev. B*, 2014, **89**, 125411.
51. D. K. Efetov and P. Kim, *Phys. Rev. Lett.*, 2010, **105**, 256805.

**Table 1**

Structural and energetic parameters of carbon nitride lattices: Bond length of C-N bonds ( $d_{C-N}$ ), bond angle between two C-N bonds ( $\angle C-N-C$ ) in s-triazine ring, lattice constant ( $a$ ) and formation energy ( $\Delta E$ ).

<i>Lattices</i>	$d_{C-N}$ (Å)	$\angle C-N-C$ (°)	$a$ (Å)	$\Delta E$ (eV/atom)	
				N-rich	C-rich
g-C <sub>3</sub> N <sub>4</sub>	1.327	116.1	4.785	0	0
g-C <sub>4</sub> N <sub>3</sub>	1.349	120.9	4.833	-0.006	0.194
g-C <sub>6</sub> N <sub>6</sub>	1.340	114.4	7.119	-0.108	-0.008

## Figure captions

### Fig.1

(a) Schematic representation of the s-triazine based  $g\text{-C}_3\text{N}_4$ , whose precursor (Melamine) is also presented. (b) Schematic representation of the honeycomb lattice of s-triazines ( $g\text{-C}_6\text{N}_6$ ). The unit cell is indicated by the yellow shaded area with the two basis vectors of  $\mathbf{a}_1$  and  $\mathbf{a}_2$ . (c) Phonon spectrum of  $g\text{-C}_6\text{N}_6$  along the high symmetric points in BZ. Brillouin zone and high symmetric points were also presented. (d) A possible scheme for the synthesis of the  $g\text{-C}_6\text{N}_6$  lattice by the reaction of cyanuric chloride with sodium metal.

### Fig.2

Simulated XRD patterns of the three graphitic carbon nitride materials:  $g\text{-C}_3\text{N}_4$  (top),  $g\text{-C}_4\text{N}_3$  (middle) and  $g\text{-C}_6\text{N}_6$  (down).

### Fig.3

(a) Electronic band lines (without SOC) of  $g\text{-C}_6\text{N}_6$  in proximity of the Fermi level (set to zero) along the high symmetric points in BZ. Four  $p_{x,y}$ -orbital bands are indicated by the green solid lines in order to distinguish with other bands. The data of our TB model is indicated by the red dotted lines. (b) The electronic density of states (PDOS) projected on to the  $s$ ,  $p_x$ ,  $p_y$  and  $p_z$  atomic orbitals of C and N atoms. The energy at the Fermi level is set to zero. (c) Enlarged view of the four  $p_{x,y}$  bands with remarkable SOC band gaps. (d) The isosurfaces of the Kohn-Sham wave functions of the four  $p_{x,y}$  bands nearest to the Fermi level with an isovalue of  $0.03 \text{ \AA}^{-3}$ . Nearest neighbor hopping within a s-triazine ring ( $t$ ) and between adjacent s-triazines ( $\gamma$ ) are also indicated.

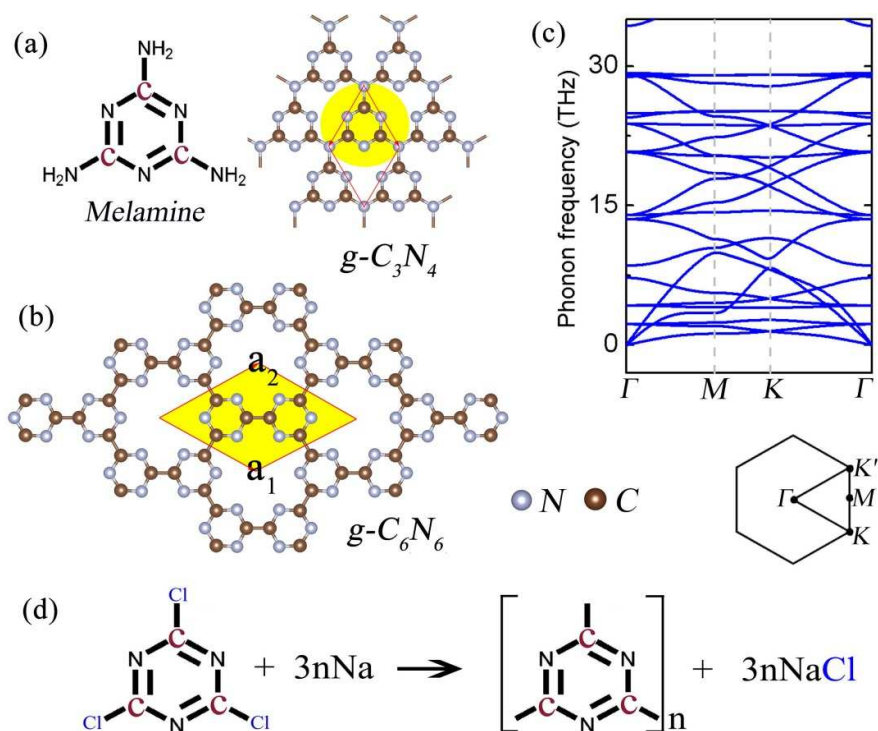
### Fig.4

Brillouin zone with the values of  $\delta_i$  associated with the time-reversal invariant momenta. (a) SOC gap ( $\Delta_1$ ) between the top flat band and the top Dirac band, (b)

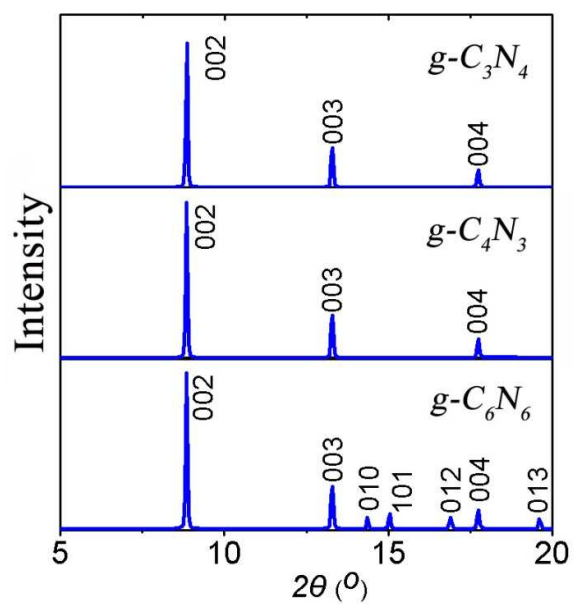
SOC gap ( $\Delta_2$ ) between the two Dirac bands. The basis vectors of the reciprocal lattice are indicated by  $\mathbf{b}_1$  and  $\mathbf{b}_2$ .

**Fig.5**

Schematic representations of honeycomb lattices of (a)  $g\text{-C}_{12}\text{N}_6$  and (b)  $g\text{-C}_{24}\text{N}_6\text{H}_{12}$ . Unit cells are indicated by the yellow shaded area. The electronic band structures are shown in corresponding right panel. The enlarged view of top four valence bands of  $g\text{-C}_{24}\text{N}_6\text{H}_{12}$  lattice are indicated by green solid lines here. Carbon atoms in difference chemical environments (C1, C2, and C3) are represented by the balls in different colors.

**Fig.1**

(a) Schematic representation of the s-triazine based g-C<sub>3</sub>N<sub>4</sub>, whose precursor (Melamine) is also presented. (b) Schematic representation of the honeycomb lattice of s-triazines (g-C<sub>6</sub>N<sub>6</sub>). The unit cell is indicated by the yellow shaded area with the two basis vectors of  $\mathbf{a}_1$  and  $\mathbf{a}_2$ . (c) Phonon spectrum of g-C<sub>6</sub>N<sub>6</sub> along the high symmetric points in BZ. Brillouin zone and high symmetric points were also presented. (d) A possible scheme for the synthesis of the g-C<sub>6</sub>N<sub>6</sub> lattice by the reaction of cyanuric chloride with sodium metal.

**Fig.2**

Simulated XRD patterns of the three graphitic carbon nitride materials:  $g\text{-C}_3\text{N}_4$  (top),  $g\text{-C}_4\text{N}_3$  (middle) and  $g\text{-C}_6\text{N}_6$  (down).

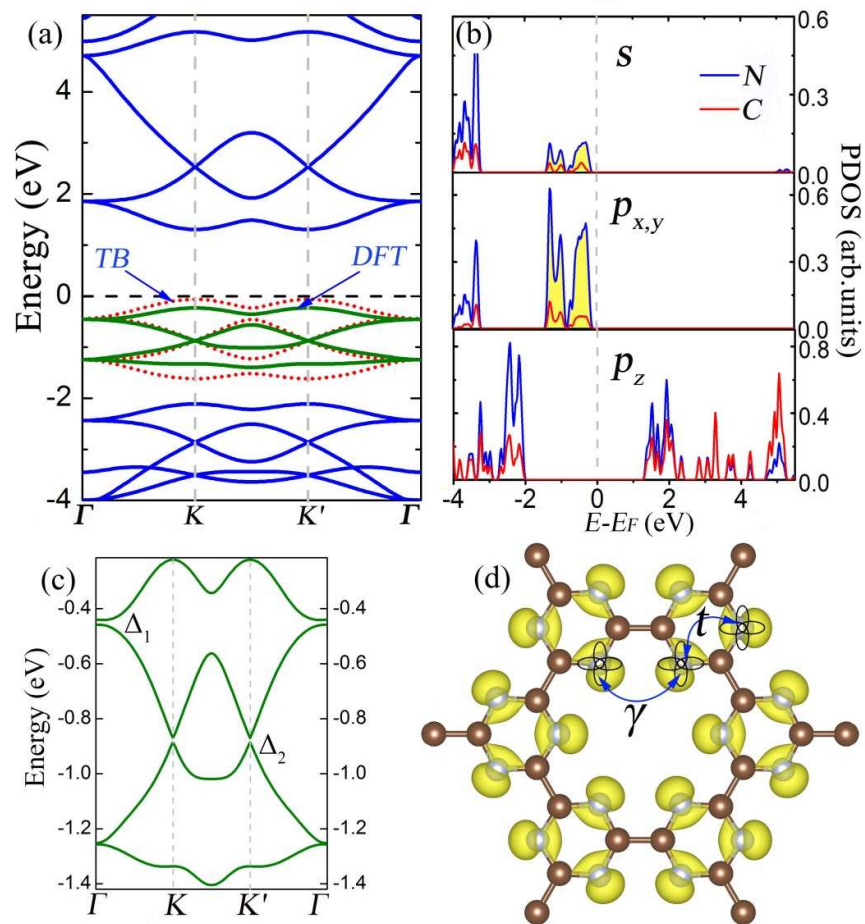


**Fig.3**

(a) Electronic band lines (without SOC) of g-C<sub>6</sub>N<sub>6</sub> in proximity of the Fermi level (set to zero) along the high symmetric points in BZ. Four  $p_{x,y}$ -orbital bands are indicated by the green solid lines in order to distinguish with other bands. The data of our TB model is indicated by the red dotted lines. (b) The electronic density of states (PDOS) projected on to the  $s$ ,  $p_x$ ,  $p_y$  and  $p_z$  atomic orbitals of C and N atoms. The energy at the Fermi level is set to zero. (c) Enlarged view of the four  $p_{x,y}$  bands with remarkable SOC band gaps. (d) The isosurfaces of the Kohn-Sham wave functions of the four  $p_{x,y}$  bands nearest to the Fermi level with an isovalue of  $0.03 \text{ \AA}^{-3}$ . Nearest neighbor hopping within a s-triazine ring ( $t$ ) and between adjacent s-triazines ( $\gamma$ ) are also indicated.

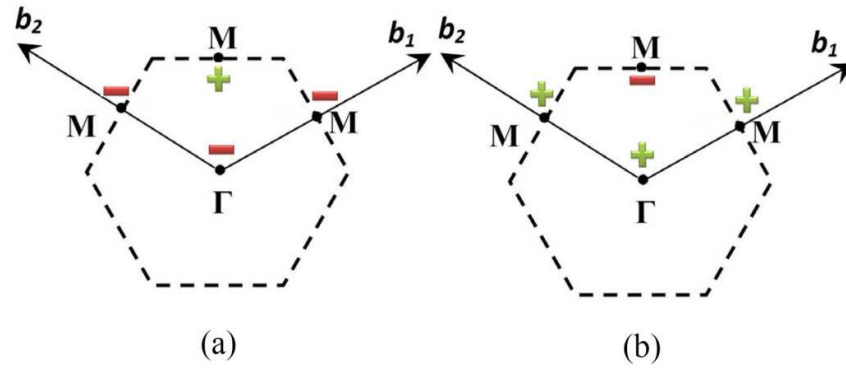


**Fig.4**

Brillouin zone with the values of  $\delta_i$  associated with the time-reversal invariant momenta. (a) SOC gap ( $\Delta_1$ ) between the top flat band and the top Dirac band, (b) SOC gap ( $\Delta_2$ ) between the two Dirac bands. The basis vectors of the reciprocal lattice are indicated by  $b_1$  and  $b_2$ .

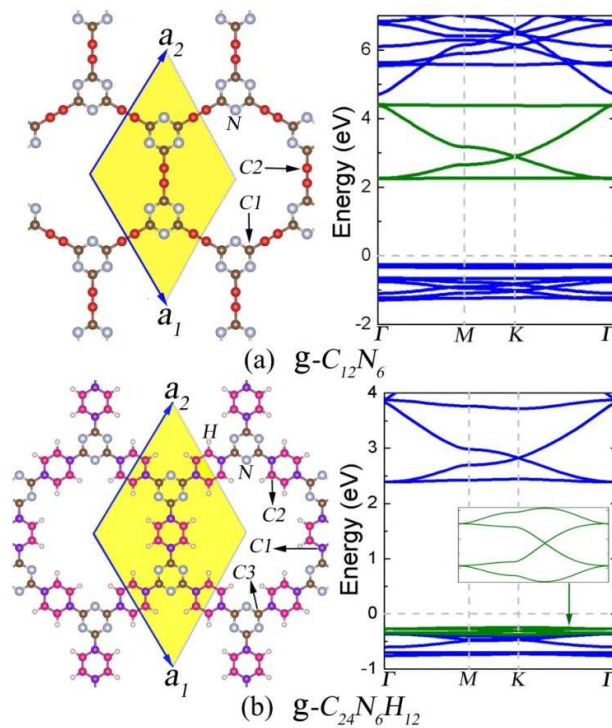


**Fig.5**

Schematic representations of honeycomb lattices of (a)  $g\text{-C}_{12}\text{N}_6$  and (b)  $g\text{-C}_{24}\text{N}_6\text{H}_{12}$ . Unit cells are indicated by the yellow shaded area. The electronic band structures are shown in corresponding right panel. The enlarged view of top four valence bands of  $g\text{-C}_{24}\text{N}_6\text{H}_{12}$  lattice are indicated by green solid lines here. Carbon atoms in difference chemical environments (C1, C2, and C3) are represented by the balls in different colors.